



Mathematical analysis of the Accordion Grating illusion: A differential geometry approach to introduce the 3D aperture problem

Arash Yazdanbakhsh^{a,b,*}, Simone Gori^{c,d}

^a Cognitive and Neural Systems Department, Boston University, MA, 02215, United States

^b Neurobiology Department, Harvard Medical School, Boston, MA, 02115, United States

^c Università degli studi di Padova, Dipartimento di Psicologia Generale, Via Venezia 8, 35131 Padova, Italy

^d Developmental Neuropsychology Unit, Scientific Institute "E. Medea", Bosisio Parini, Lecco, Italy

ARTICLE INFO

Keywords:

Visual illusion
Motion
Projection line
Line of sight
Accordion Grating
Aperture problem
Differential geometry

ABSTRACT

When an observer moves towards a square-wave grating display, a non-rigid distortion of the pattern occurs in which the stripes bulge and expand perpendicularly to their orientation; these effects reverse when the observer moves away. Such distortions present a new problem beyond the classical aperture problem faced by visual motion detectors, one we describe as a 3D aperture problem as it incorporates depth signals. We applied differential geometry to obtain a closed form solution to characterize the fluid distortion of the stripes. Our solution replicates the perceptual distortions and enabled us to design a nulling experiment to distinguish our 3D aperture solution from other candidate mechanisms (see Gori et al. (in this issue)). We suggest that our approach may generalize to other motion illusions visible in 2D displays.

© 2011 Elsevier Ltd. All rights reserved.

1. Introduction

A new visual illusion discovered by one of the authors (S.G.) is reported here. A simple observation shows a perceived deformation from densely juxtaposed parallel lines while moving toward and away from it. This pattern presents two illusory effects: (1) Moving toward and away from the grating creates an expansion/contraction of the stimulus frame perpendicular to the stripes but not parallel with the stripes. One can notice it by paying attention to the stimulus outline in Fig. 1 and observing a horizontal expansion/contraction and less or negligible vertical expansion/contraction. This illusory effect is less vivid than the Rotating Tilted Line Illusion (Gori & Hamburger, 2006) in which a clear rotation emerges. During the observation of the illusion, a loss of the stripes' rigidity (fluid distortion) is observed and the stripes look curved as a function of the observer's motion which is the focus of the present analysis. Foster and Altschuler (2001) reported distortion for a checkerboard grid being viewed by the subject in a back and forth head movement, with the difference being that they used a checkerboard pattern that has many intersections. In the mathematical analysis of our present stimulus, there is no

need for line-ends or intersections along the lines to explain the illusion. In fact, our analysis shows that adding more and more intersections systematically decreases the original illusory effect as experimentally shown in Gori et al. (in this issue).

The combination of these phenomenal distortions is similar to the deformations of an accordion while being played, and originated the name of the illusion: the Accordion Grating (AG).

The simple geometrical design of the stimulus renders it a suitable substrate for mathematical analysis (Fig. 1).

This phenomenon is interesting because long lines have no singularities except the line-ends. Having few singularities turned out to be a useful characteristic for the stimuli used in motion analysis (Adelson & Movshon, 1982; Fennema & Thompson, 1979; Grossberg & Mingolla, 1993). Data from single cell electrophysiology shows a delayed true coherent motion signal detection for the mid-portion of long lines, which originates from the motion signals of the line-ends (Pack & Born, 2001).

Without getting into the complexities of binocular vision, we would like to analyze the situation for the monocular condition and see how much of the illusion is predictable based on the geometry of light projection as well as the motion processing units' properties. The result can then be used as a basis to analyze further deviation from it, and uncover other possible factors involved.

2. Stimulus configuration

Although the original stimulus design is based on head movement toward and away from the stimulus with a fixed size,

* Corresponding author at: Cognitive and Neural Systems Department, Boston University, MA, 02215, United States.

E-mail addresses: yazdan@bu.edu (A. Yazdanbakhsh), simone.gori@unipd.it (S. Gori).

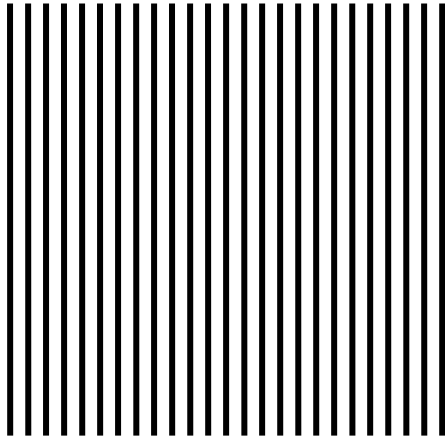


Fig. 1. The stimulus of the Accordion Grating. The stimulus is composed of densely juxtaposed parallel lines. Moving toward and away from the stimulus rapidly makes it look as if it centrally bulges and contracts respectively, hence the name, Accordion Grating illusion. The stimulus has a unique design, while its illusory effect is vivid, its geometrical structure is very simple – parallel lines – which makes it a useful candidate for a differential geometry analysis.

in the present study we based our analysis on the fixed position of the head and monitor using, instead, a uniform expansion and contraction of the stimulus. This approach is beneficial, because the presentation is replicable and there is no need to deal with head movement variation across subjects. In fact, a fixed amount of expansion and contraction with a fixed distance from monitor can be replicated in different labs for consistency. Such an approach has been successfully tested in a previous work with Rotating Tilted Line Illusion (RTLI) (Yazdanbakhsh & Gori, 2008) while the very original version of RTLI has a head movement involved (Gori & Hamburger, 2006; Gori & Yazdanbakhsh, 2008). In the few next analysis sections, this fixed distance is represented by d which is constant over time for each condition, but differs for different conditions.

The pattern of grating expansion is shown in Fig. 2. As can be seen, it has a radial pattern as if one prints the stimulus on an elastic sheet and then the sheet expands/contracts radially. Each point of the stimulus is expanded proportional to the distance from the center. As mentioned, this is instead of having the head move toward/away from the stimulus to produce the same radial expansion over the retina.

3. Problem formulation

To start approaching the nature of the illusion, we assume the observer’s eye nodal point (O) has a distance $OO' = d$ from the stimulus center (O') where the stimulus is centered at the base of the vertical line of sight (Fig. 3). We index the central bar of stimulus which passes over O' zero ($n = 0$). The parallel lines to its right are indexed positively ($n = 1, 2, 3 \dots$) and to its left indexed negatively ($n = -1, -2, -3 \dots$). The line passing through O' and orthogonal to parallel lines is called Ov or $x = 0$ line (Fig. 3). Along each of the parallel lines, the distance from the $x = 0$ line is denoted by x (positive on top of $x = 0$ and negative at the bottom). The number of the bars are set to be odd to keep the symmetry ($n = -10 \dots 10$). For each point of the stimulus A, OA is a projection line.

To evaluate the projection line from each point of the stimulus to the eye’s nodal point (O), we consider a point (A) located over the n th bar and being offset from the mid perpendicular line by the amount x (Fig. 3). Because the distance between the consecutive parallel lines is a , the coordinate of A is therefore (na, x) .

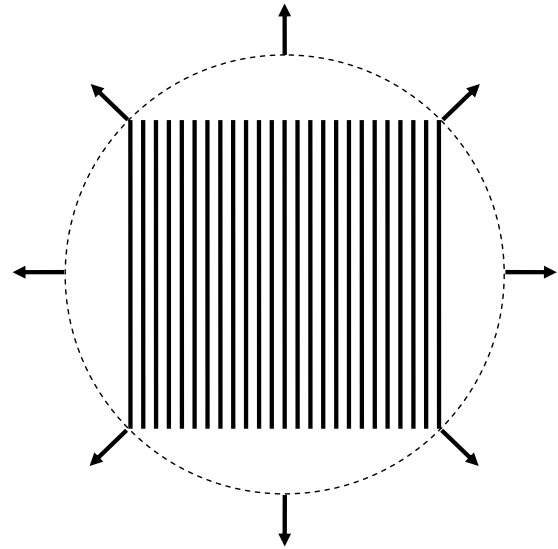


Fig. 2. Expanding motion of the AG pattern: each point of the stimulus is expanding proportional to the distance from the center of the expansion.

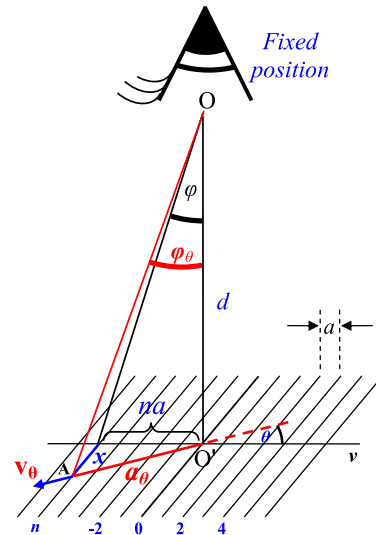


Fig. 3. Eye and stimulus position. Fixed position of the eye nodal point (O) and a line of sight perpendicular to the stimulus plane (OO'), in which O' is set to be the center of the middle line of the stimulus (indexed by $n = 0$). The parallel lines to the right of the $n = 0$ line are indexed by $n = 1, 2, \dots, 10$ and to the left by $n = -1, -2, \dots, -10$. The perpendicular line passing through O' is called the $x = 0$ line or Ov . For each point of the stimulus A, OA is a projection line.

3.1. Classical aperture problem

If a motion processing unit does not encompass the line-ends or any signal related to them, then the detector is said to have an aperture problem (Gurnsey et al., 2002; Lorenceau et al., 1993; Stumpf, 1911; Wallach, 1935) (Fig. 4(a)). In this case, the motion processing unit can only detect the component of motion perpendicular to the line orientation. Instead, Fig. 4(b) shows the condition in which the line-ends are within the aperture and the true direction of motion can be detected.

3.2. Can the classical aperture problem explain the fluid distortion?

Fig. 5 shows the classical aperture problem analysis of the stimulus. Let us again consider an arbitrary point A over the n th stimulus line from the center. Due to isotropical expansion, the n th line speed or the speed of point A' (image of A over the line $x = 0$)

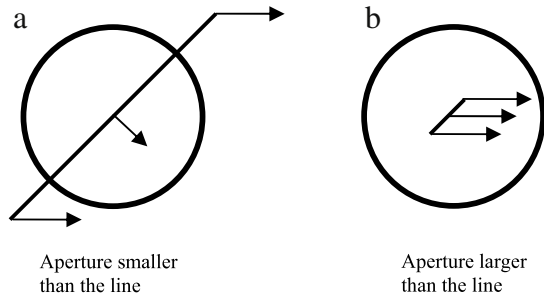


Fig. 4. If one considers the motion processing unit receptive field as an aperture to the visual field, the long lines fool the motion unit (a) and the short lines do not (b). In (a) the motion registered by the unit through the aperture is orthogonal to the orientation of the line and in (b) is parallel with the true direction of motion. It is obvious that there is a third case, in which only one line-end is in the aperture. But in that case the line can be very long, and still, there is no aperture problem, hence it is not the length of the line but rather the position of its terminator that matters.

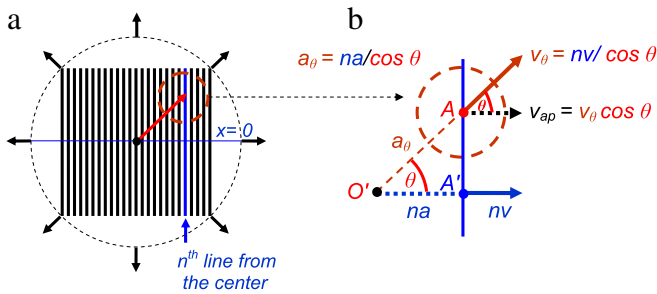


Fig. 5. The classical aperture problem cannot explain the fluid distortion. (a) Consider an aperture over the stimuli (red dotted circle). In (b) the aperture is zoomed. Due to the isotropical/radial expansion/contraction, the ratio of radial speed of point A (v_θ) to its projection over the horizontal line (blue) is equal to the ratio of the corresponding distances from the stimulus center (O), or $a_\theta/na = 1/\cos\theta$, hence $v_\theta = nv/\cos\theta$ and its aperture component is $v_{ap} = v_\theta \cos\theta = nv$. Therefore, the classical aperture problem predicts the same speed perpendicular to the line orientation ($v_{ap} = nv$) throughout the line, which does not indicate the loss of rigidity or fluid distortion: it rather predicts a solid displacement.

equals nv , in which v is the relative speed of two consecutive lines. For the same reason, the real speed of point A (v_θ) compared to the speed of A' (nv) scales up by the factor of $1/\cos\theta$ (the angle θ is between $O'A$ and $O'A'$) and hence v_θ equals $nv/\cos\theta$ (Fig. 5).

However, through the red dotted aperture around A, only the normal (perpendicular to line orientation) component of v_θ is detectable (classical or 2D aperture problem). This normal component (v_{ap}) equals $v_\theta \cos\theta$. Because $v_\theta = nv/\cos\theta$, as a result, v_{ap} equals nv . This chain of calculation which goes clockwise with reference to the right panel of Fig. 5, starting from $O'A'$, provides the proof that the aperture problem, known classically in the literature, and from now on we refer to it as the classical or 2D aperture problem, cannot explain the fluid distortion of the lines. The result of the calculation shows that the aperture speeds of all the points along the stimulus line are equal (nv) to leave no substrate for distortion. The part of illusion predictable by the classical/2D aperture problem is the horizontal expansion of lines (with the amount of nv for each line) and the less or absence of vertical elongation of lines (parallel to the lines' orientation). In summary, the classical aperture problem explains the aspect ratio modulation of the accordion grating illusion (widening) (Gori et al., in this issue) but not the fluid distortion of it.

This situation motivated the formulation of the problem beyond the classical aperture problem and led to the introduction of the concept of the 3-dimensional (3D) aperture problem, based on the projection line analysis and angular speed. In the following section, such a formulation is presented and the concept of the 3D aperture problem is introduced.

3.3. Beyond the classical aperture problem: 3D aperture problem, incorporating the projection line

Noticing that the classical or 2D aperture problem can only explain the aspect ratio distortion and cannot account for the fluid distortion, we introduce and formulate another source of ambiguity in interpreting the projection line through the eye's nodal point. As can be seen, not only does the 2D or classical aperture problem influence the formulation, but also another component, based on the projection line and its relation with the stimulus plane contributes in the ambiguity of motion detection. Such a source of ambiguity, related to the projection line and its angle with the stimulus plan has an extra dimension beyond the 2D aperture on the stimulus plane and extends in 3D visual space between the eye and stimulus. Therefore the "3D Aperture Problem" denotes the ambiguity emergent from the contribution of all 3 dimensions of visual space. In short, the 3D aperture problem can be defined as the ambiguity of true direction of motion faced by a motion detector due to a limited 2D aperture view and the relation of the projection line with the stimulus plane. Corresponding to the 2D aperture problem, which occurs when a sensor needs 2D information to resolve the stimulus but only has access to 1D information, we define a 3D aperture problem, which occurs when three dimensions of information are needed but only two are presented.

In the present case, the third dimension is depth, which is poorly specified by the 2D grating, despite its physical flatness. The visual system needs to estimate possible motions in all three planes, but the receptive fields at the ends of the bars only have access to 2D information.

The next section shows that the inclusion of this extra dimension yields less registration of motion further away from the line centers which collectively creates the impression of a fluid distortion.

3.4. Formulation of 3D aperture problem

Consider the projection line OA (Fig. 6). This line makes an angle φ_θ with the vertical line $O'O$. To get a handle on φ_θ for calculating the angular speed of the projection line, we consider:

$$\text{tg } \varphi_\theta = \frac{a_\theta}{d} = \frac{na}{d \cos \theta} = \frac{n}{d} \left(\frac{a}{\cos \theta} \right), \quad (1)$$

which paves the path for calculating the angular speed or $\frac{d\varphi_\theta}{dt}$ by calculating $\frac{d \text{tg } \varphi_\theta}{dt}$. This can be done in two different ways: considering the absence or presence of the classical/2D aperture problem.

Appendix A shows that for the 3D aperture problem, the presence of the 2D aperture problem is necessary. If the true (radial) motion of point A is detected, there is no 2D aperture problem and the component of motion perpendicular to the line orientation (v_\perp) then equals nv (see Appendix A). We therefore only consider motion processing units that face the 2D aperture problem.

The next section derives the configuration of the 3D aperture problem in the presence of its 2D precursor.

3.5. Projection line analysis with the presence of the 2D aperture problem: formulating the 3D aperture problem

At this point we consider the presence of the 2D aperture problem in the neighborhood around point A and will follow the same framework of calculations as in Appendix A and the previous section to see whether v_\perp remains equal to nv or not.

Given the 2D aperture problem, θ must vary (Fig. 6, also compare it with Fig. 3), because the x coordinate of the motion of

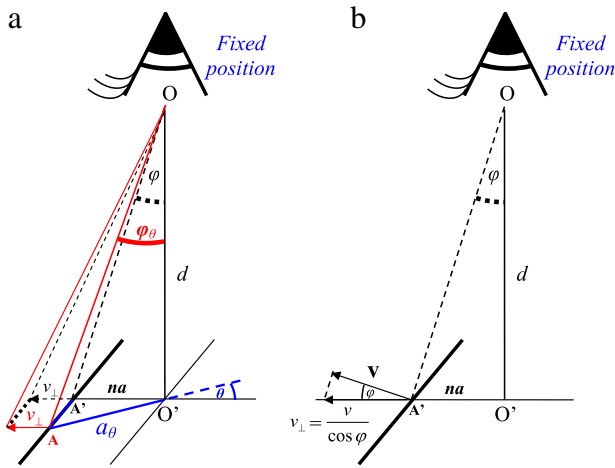


Fig. 6. Aperture problem assumption. Only the perpendicular component v_{\perp} is detectable (red). Parallel and equal to it, over line $x = 0$, v_{\perp} is projected (dotted, black). In panel (b), the plane containing $O'OA'$ (from panel a) is shown to facilitate the calculation of angular speed. (For interpretation of the references to colour in this figure legend, the reader is referred to the web version of this article.)

a bar along its length, when seen through a 2D aperture remains constant.

Hence, we re-write (1) in terms of x to separate the constant and variable terms:

$$tg\varphi_{\theta} = \frac{a_{\theta}}{d} = \frac{\sqrt{n^2 a^2 + x^2}}{d}. \tag{2}$$

As derived in Appendix B, this time, the component of motion perpendicular to line orientation (v_{\perp}) is:

$$v_{\perp} = nv f^{Ap}(n, x), \tag{3}$$

where,

$$f^{Ap}(n, x) = \frac{na\sqrt{n^2 a^2 + d^2}}{\sqrt{n^2 a^2 + x^2} \sqrt{x^2 + n^2 a^2 + d^2}}, \tag{4}$$

indicating the distortion function under the aperture problem assumption (f^{Ap}) systematically deviates from one in terms of n and x .

The shape of the function can best be realized by a graph which plots $v_{\perp} = nv f^{Ap}(n, x)$ along abscissa against x on the ordinate to be consistent with the way x is defined in Fig. 3. To make this graph visually intuitive and consistent with the distortion prediction it provides, we can fix d and draw the graph for each n ($-10, 9, \dots, 0, 9, 10$) separately and put them side by side in the same way that stimulus lines are side by side (see the extensive treatment of this in Figs. 9 and 10 with different parameter choices in the next sections).

An intuitive account of the 3D aperture problem, which is analytically described in (4) involves the underestimation of v_{\perp} originating from the projection lines not perpendicular to the stimulus plane and its lines. Further intuitions are described in the next section.

3.6. An intuitive description of the 3D aperture problem outcome

Regarding (3) and (4), by increasing n for a fixed value of x , the fraction $\frac{na\sqrt{n^2 a^2 + d^2}}{\sqrt{n^2 a^2 + x^2} \sqrt{x^2 + n^2 a^2 + d^2}}$ gets closer to one, or closer to the predicted speed at $x = 0$ (nv). This provides a better understanding of the curvature decrement by increasing n . Fig. 7 is hand drawn to show the situation for two different n 's to illustrate the effect qualitatively.

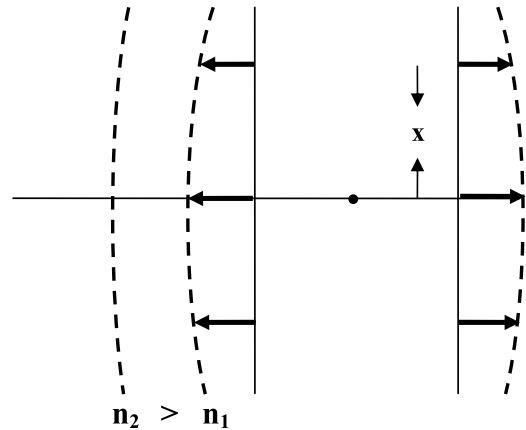


Fig. 7. The effect of a larger n on decreasing the distortion due to its contribution on closer-to-veridical motion detection along the entire line based on Eq. (4). With the larger n , the change in x has less effect on deviating the perceived motion from the veridical value nv (Eqs. (3) and (4)) and therefore the distortion is less (see also Figs. 9 and 10).

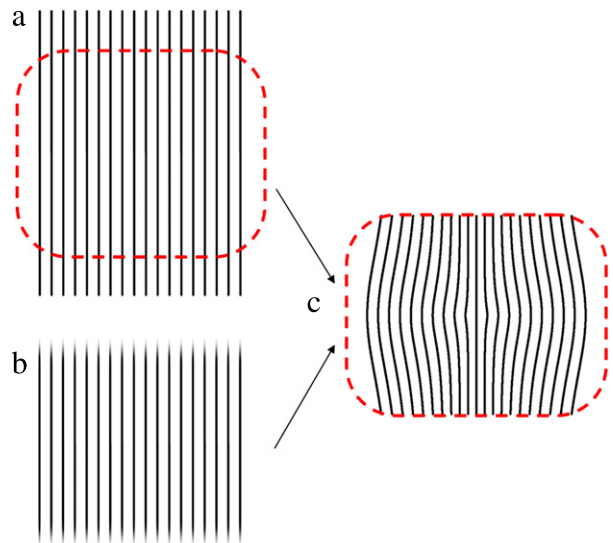


Fig. 8. The target region of the stimulus for analysis. Mid-segments of longer lines (a), or the stimulus with blurred line-ends to make the line-end signal weak (see the text). These are candidate conditions through which we based our analysis and graph generation (c).

As can be seen, for a stimulus line farther from the center ($n_2 > n_1$), the decrement of displacement from the veridical is less. Hence the closer the stimulus line to the center, the more curved it appears.

3.7. How can blurring contribute to the illusion?

The resulting pattern of the illusion from (4), which is the outcome of 3D aperture problem, requires the presence of the classical/2D aperture problem and this excludes the regions close to the line-ends, which naturally do not suffer from the 2D aperture problem. In this sense, all of the predicted displacements by Eqs. (3) and (4) can be attributed to the mid-portion of the stimulus far from the line-ends as highlighted by a dotted red outline (Fig. 8(a)).

Downgrading the line-ends, and thus their signal for the true direction of motion can also be accomplished by blurring the line-ends (Fig. 8(b)). We tested two separate sets of the stimuli; one set consisted of AG stimuli with the sharp line-ends and the other set with the blurred line-ends. All of the stimuli were smaller than the

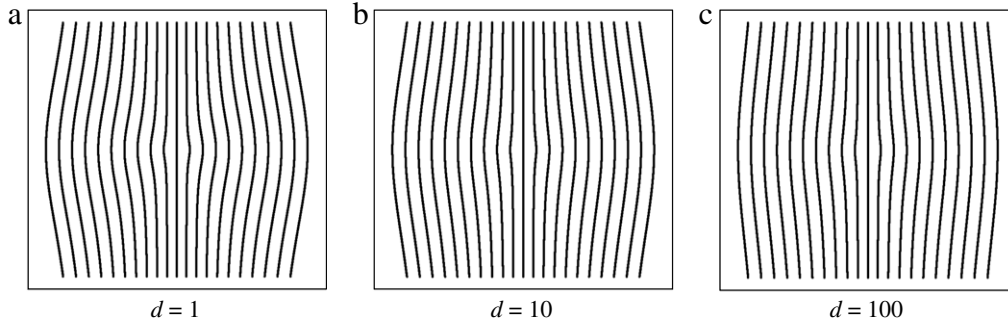


Fig. 9. The predicted pattern of the illusion for $d = 1, 10$ and 100 obtained by Eqs. (3) and (4).

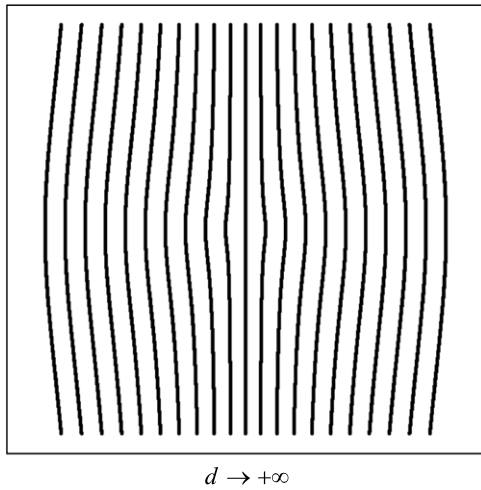


Fig. 10. Limit condition for $d \rightarrow +\infty$ obtained analytically. As can be seen, the illusion is predicted not to vanish as the subject's distance increases. Compared to the smaller value of d (Fig. 9(a)), the predicted curvature of the illusion is less and rather spans throughout the lines.

full screen. It turned out, with the blurred line-ends, the stimulus level to null is higher (Gori et al., in this issue).

On the other hand, blurring the line-ends can influence the illusion by decreasing the blurred part contrast with the background and causing the velocity near the line-ends to appear less. We showed that in fact this is the blurring rather than contrast decrement which contributes to the reduced line-end signal to enhance the illusion strength (Gori et al., in this issue).

3.8. Further insight into the illusion emergent from the 3D aperture problem

For $x = 0$ the function $f^{Ap}(n, x) = 1$, which means a veridical registration of nv , but as soon as x deviates from 0 (mid-point of each line) toward positive or negative values, $f^{Ap}(n, x) < 1$, which means the v_{\perp} gets less and less than nv (Fig. 7). This is congruent with the illusion direction, where the lines bulge out in their mid-region compared to line-ends. This bulging is predicted to have a continuous and flowing nature because for any x_1 and x_2 , when $|x_1| < |x_2|$, $f^{Ap}(n, x_1) > f^{Ap}(n, x_2)$, an indication that $f^{Ap}(n, x)$ is a monotonic decreasing function in terms of $|x|$. The monotonic decrement is less when n is larger (Fig. 7).

3.9. A few parameter choices for further insight

As a demonstration of the speed field, we show a few examples for different parameters. As can be seen in Fig. 9, 21 parallel lines are chosen, 10 to the left and 10 to the right of the central one ($-10 < n < 10$). The distance between the consecutive lines is

set to be 1 ($a = 1$), hence the width of stimulus on each side of the central line is $10a = 10$ (total width $2 \times 10 = 20$). To make the stimulus outline square, we chose the line length 20 equal to the stimulus width ($x_{max} = 10$ for $-x_{max} < x < x_{max}$).

Also for the present examples, we choose $v = 1$ and keep in mind that changing v merely scales the amount of v_{\perp} , because as (3) and (4) show, v appears in the numerator once and $f^{Ap}(n, x)$ is invariant against v . To better understand the effect of distance d on the predicted distortion, Fig. 9(a)–(c) show examples for $d = 1, 10, 100$ respectively. We chose $d = 10$ to be comparable to the lines' length or the stimulus outline. To evaluate the effect of viewing distance when it is one order of magnitude more or less than the stimulus size, we chose $d = 100$ and 1, respectively (Fig. 9).

The graphs in Fig. 9 are generated by shifting horizontally each point of the n th line with coordinate x by the amount obtained from $v_{\perp}(n, x) \times \Delta t$ (for $\Delta t = 0.3$).

It can be seen that in all the above distance values d , the predicted fluid distortion exists and does not vanish, in particular, in the very close or far distances.

In the three examples of Fig. 9, the curvature of the central lines vanishes to straight lines closer to their mid-point, compared to peripheral lines, where the curvature extends longer (Fig. 7). This can explain the illusions' appearance as a bulging spherical distortion.

3.10. Further insight into the predicted fluid distortion

Limit conditions provide further qualitative impression of the illusion appearance. We investigate three limit cases:

- (1) $\lim x \rightarrow 0$

From (3) and (4) it can be directly obtained:

$$\lim_{x \rightarrow 0} v_{\perp}(n, x) = nv,$$

which indicates that independent from distance d , for $x = 0$ the speed detection is congruent with the real speed and is at its maximum value. As (4) shows, as soon as x deviates from zero, $f^{Ap}(n, x)$ and the predicted speed decreases.

- (2) When the central line is considered ($n = 0$):

This condition can take place only when the total number of parallel lines is odd, and therefore, the stimulus has the central line with $n = 0$. From (4) it can be obtained directly:

$$v_{\perp} = nv = 0.v = 0.$$

The result reflects no distortion for the central bar. This can also be deduced directly from the concept of symmetry, because any result besides $v_{\perp} = 0$ means that the central bar would split in the center, which is not the case. On the other hand, for an even number of total bars, $n = 1$ and $n = -1$ represents the immediate right and left bars with respect to the fixation point with symmetrical distortions.

(3) $\lim d \rightarrow \infty$

In other words, we are interested to know what could be obtained from (4) when the subject gets far away from the stimulus; in particular does the illusion vanish?

The terms containing d in (4) can be segregated:

$$f^{Ap}(n, x) = \frac{na}{\sqrt{n^2a^2 + x^2}} \left(\frac{\sqrt{n^2a^2 + d^2}}{\sqrt{x^2 + n^2a^2 + d^2}} \right).$$

Regarding that, $\lim_{d \rightarrow +\infty} \frac{\sqrt{n^2a^2 + d^2}}{\sqrt{x^2 + n^2a^2 + d^2}} = 1$, it can be concluded:

$$\lim_{d \rightarrow +\infty} f^{Ap}(n, x) = \frac{na}{\sqrt{n^2a^2 + x^2}},$$

and therefore:

$$\lim_{d \rightarrow +\infty} v_{\perp} = nv \frac{na}{\sqrt{n^2a^2 + x^2}}. \quad (5)$$

The above situation is shown graphically in Fig. 10.

Therefore analysis shows that the illusion resists large viewing distances and by moving away from the stimulus, one cannot eliminate the effect.

3.11. Remark on large viewing distance and the persistence of the fluid distortion

In reality, the receptive field of each motion detector unit constitutes a portion of the visual field, rather than being an infinitesimal point.

The above analysis shows that the illusion is preserved for every d . The problem is that with the increasing of d , the projection of the calculated distortion or segments of stimulus like a or x_0 in terms of “visual angle” become negligible with respect to a realistic receptive field size. This explains why the illusion cannot be perceived after a certain viewing distance. In the analysis, step one was to transform linear distances like na , a_{θ} (or $O'A$ in Figs. 3 and 6) to the corresponding visual angles, φ and φ_{θ} , and then step two was to transform them back to the linear distance and velocity, like v_{\perp} . However, subtle differences in step 1 vanish after distances (d) increase beyond a certain bound, leaving no hint to be transferred back in step two; a sampling theorem related topic.

Therefore, the analysis holds as long as the viewing distance d is small enough to let the calculated distortion in (4) generate a visual angle resolvable by the receptive field and grouping processes (denoted by d_{\max}). Beyond d_{\max} , to maintain the illusion, the stimulus should be enlarged to make a resolvable angular substrate to be registered in step one; again, a sampling theorem related topic.

3.12. Designing a nulling paradigm

If one inverts the distortion function in (4) within practical distances (d) and speeds (v) for subjects it can be seen whether, nulling is under- or over-compensating the perceived distortion. The practical measures we used to test the subjects are summarized in the following:

The stimuli were a series of movies with gratings increasing from 9.4 to 9.8 cm. Four independent variables were manipulated: (1) Five levels of inverted curvature (by inverting the numerator and denominator in distortion function of Eq. (4)) were applied with 0 for no inverted distortion or plain AG stimulus (nulling stimulus level 0), and 4 for full inverted distortion (nulling stimulus level 4). All other nulling stimuli levels in between 0 and 4 (nulling stimuli levels 1–3) are obtained by linear interpolation. (2) The movies were prepared for 5 distances from the screen: 15, 25, 35, 45 and 55 cm. (3) Five speeds (v) were used: 1.2,

2.4, 3.6, 4.8, 6.0 mm/s. (4) Two gratings, one with sharp line-end boundaries and one with Gaussian blurred line-ends were tested (Gori et al., in this issue). Our results show that the faster the expansion/contraction, the higher the stimulus level needed to null the distortion, which is consistent with the fact that the neural substrate needed to correct the distortion takes time. The data confirm the presence of fluid distortion in the range of distances: the closer the viewing distance, the higher the level of stimulus to null the distortion. With respect to the blurring of line-ends, the data show the stimuli with higher levels null the distortion, consistent with the idea that either the lower contrast of the line-ends or their blurring reduces the influence of the end-stopped units. In the following Discussion section we offer an explanation on how these findings can contribute in experimental and modeling domains.

4. Discussion and conclusion

The Accordion Grating illusion generates a percept of elastic outward bulging and contraction although it is composed of parallel lines which have isotropic expansion and contraction. The well-defined geometrical pattern of the Accordion Grating illusion rendered it a very suitable substrate for differential geometry analysis. Other visual illusions were already investigated by relating the empirical results to the model assumptions (Fermuller et al., 1997). In the present work, we demonstrated a few properties of the illusion that can be obtained by the projection line analysis. These properties which are summarized in the following were tested by using the closed form solutions (3)–(4) under a nulling paradigm (Gori et al., in this issue):

1. Bulging, limited rather to the mid-zone of the central lines and more extended in the peripheral lines, creates a global impression of a wave flowing from center to the periphery.
2. Obtaining the full predicted curvature either when the line-ends are blurred or the mid-zone of the parallel lines is considered (weak line-end signal conditions).
3. The illusion theoretically persists even for a large viewing distance.
4. The bulging is related to the veridical speed perception of line centers, and less than veridical away from the centers.

In general, the introduction of the 3D aperture problem, and its prediction and the characterization of the fluid distortion, which cannot be explained by the classical/2D aperture problem, shows that besides a flat view of aperture, the angle of the projection line with the stimulus plane within 3D visual space plays a crucial role. It needs to be tested which part of the brain areas involved with motion, for example MT and MST, can incorporate the correction of the 3D aperture problem and falling behind when the stimulus speed is high.

Designing a nulling experiment based on Eqs. (3)–(4) showed the influence of the 3D aperture problem for the fluid distortion aspect of the illusion (Gori et al., in this issue). Other factors besides the classical and the 3D aperture problems could be involved in the distortion and aspect ratio change (Caplovitz et al., 2008) in particular that our nulling experiments show the perfect nulling with stimuli with less than maximum levels. As Caplovitz et al. (2008) suggested, the visual system can be faced with ambiguities other than the traditionally acknowledged aperture problem. Given that the aperture problem resulted in our closed form solution with a deformation similar to the illusion appearance of bulging, any less than predicted effect after a full nulling can reveal other factors, ambiguities, or integrative processes involved. Among the subtleties related to such an integrative process is the one discussed by Fantoni and Pinna (2008) regarding the diamond-like stimuli they used to investigate the integration of local and

global motion signals by showing motion and form attributes interact rather than being independent.

The Accordion illusion skips the compensatory neural substrate that otherwise could have corrected the deviation from the straight lines. As a result the illusion is perceived. This situation is enhanced in a fast contraction/expansion of the stimulus compared to the slower presentations (Gori et al., in this issue) indicating a time consuming compensatory mechanism. The present mathematical investigation provides a better understanding of the origin of the distortion and a straightforward candidate for experimentalists to observe which part of the brain areas can provide invariant motion detection irrespective of x and na , which may have a delayed initiation. Such a study can be considered equivalent to the experimental study of Pack and Born (2001) for the area MT, which shows that the activity of neurons are initially consistent with the motion component of the 2D aperture and after a 50 ms delay the same cell signals the corrected coherent motion. In such a suggested experimental study based on the present analysis, multiple brain areas can be tested for a delayed coherent speed detection (nv) after the initial response congruent with the underestimated value of $n.vf^{ap}(n, x)$. Within a computational modeling context, testing the time dynamics of motion detection while the model receives the input of expanding/contracting stimulus could offer a straightforward evaluation of model response. Given that the deviation from veridical speed systematically depends on x , and n , characterized directly by Eq. (4), modelers may start attempts to generate the effects as predicted by the geometrical study (Figs. 9–10). The facts that the illusory effect is enhanced with faster expansion/contraction (Gori et al., in this issue) and is dependent on viewer distance d from the stimulus (Fig. 9) impose further parametric constraints on the proposed model.

In this context, approaches to motion integration based on regularization frameworks are quite relevant. For example, formulating an additional constraint of smoothness of the velocity field, based on the physical assumption that object surfaces are generally smooth, allows the computation of a unique velocity field (Hildreth, 1984). Interestingly in our present stimulus, the predicted distortion is smooth, and does not violate this constraint, which may explain why the fluid distortion survives. Gong and Brady (1990) have suggested Structure-from-motion algorithms based on matched point-like features under orthographic projection for use in analyzing image motion from small rigid moving objects. By minimizing an energy term the smoothness of the moving outline is generated. Given the latter smoothness generation, the smooth distortion in our present illusion can survive if passed through their algorithm. Moreover, our present illusion lacks small fragments/objects to generate multiple singularities along the line (opposite to a checkerboard) which is used in the above analysis. With respect to models that assume smoothness, the bistable percept of rigidity and elasticity of the so-called gelatinous ellipses based on the overall contour curvature is relevant (Weiss & Adelson, 2000). They showed that the percept can be accounted for by a class of models that assumes smoothness in a layered representation. Again the predicted fluid distortion in the present stimulus does not violate the smoothness assumption as illustrated by our direct percept.

The phenomenological description and possible neurophysiological correlation in the illusion can complement each other in researches which seek the correlations between the percept and the possible neural activities (Grossberg, 2000; Spillmann, 2009). In conclusion, this new illusion presents useful characteristics to be described by geometry, and consequently, it helps to understand how the motion processing units of our visual system work in analyzing the visual field.

In general, stimuli with an illusion which relates to the classical aperture problem can be revisited in terms of the 3D aperture

problem, especially if the aperture elements are eccentric from the line of sight. As is clear from the present work, the difference between the predictions of the 2D and 3D aperture formulations is quantitative but not qualitative and related to the amount of perceived motion rather than its direction. For example, the rotation direction of RTLI (Gori & Yazdanbakhsh, 2008) has been predicted by the 2D aperture problem formulation. As mentioned, the 3D aperture problem will predict the same direction of rotation, but with different amounts because the RTLI stimulus can be designed with different radii which locate its elements at different eccentricities (Yazdanbakhsh & Gori, 2008). Such a difference in the predicted amount of rotation can be large enough to be measured experimentally and provide a direction for subsequent research. All illusory stimuli previously studied under the classical aperture problem can be presented in different eccentricities for testing if the amount of perceived motion is changed. This should be a general topic of interest to vision scientists studying spatial vision and those focusing on motion detectors with a limited sampling field.

Acknowledgments

Supported in part by CELEST, a National Science Foundation Science of Learning Center (NSF SBE-0354378 and OMA-0835976). We thank Ariana Tart-Zelvin and Michael-John Tavantzis for the helpful feedback on the manuscript text. Special thanks to Adam Reeves the editor of the paper and to Cynthia Bradford for the kind handling of the submission process.

Appendix A. Obtaining v_{\perp} assuming no aperture problem

By following the projection line analysis, but assuming that the motion processing units do not face the classical/2D aperture problem, we aim to provide a proof of concept, namely, our formulation of the projection line analysis is veridical and results in correct registration of motion in the absence of the classical aperture problem. After, this proof of concept, we implement our projection line formulation to characterize the 3D aperture problem in the presence of its 2D precursor.

With no classical/2D aperture problem, θ and, as a result, $\cos \theta$ and $\frac{1}{\cos \theta}$ are constant. This is because the true motion of point A is detectable (no aperture problem) and the radial expansion of point A (Fig. 3) is detected to be along the radial line OA, which assures the constancy of θ , the angle between OA and the line Ov (line of $x = 0$).

In this condition, as the following calculations show, even the projection line analysis yields no illusory distortion and the component of motion perpendicular to line orientation (v_{\perp}) is governed by:

$$v_{\perp} = nvf^{no}(n, x),$$

where, distortion function $f^{no}(n, x)$ equals 1. This means v_{\perp} replicates the original stimulus speed.

To derive the distortion function with no aperture problem assumption (f^{no}), note that θ is constant, and as a result in differentiating from both sides of (1) one can take $\frac{1}{\cos \theta}$ as a constant term, hence:

$$\frac{dtg\varphi_{\theta}}{dt} = \frac{n}{d \cos \theta} \frac{da}{dt} = \frac{nv}{d \cos \theta}. \quad (\text{A.1})$$

Given the chain rule in derivation we have:

$$\frac{dtg\varphi_{\theta}}{dt} = \frac{1}{\cos^2 \varphi_{\theta}} \frac{d\varphi_{\theta}}{dt}. \quad (\text{A.2})$$

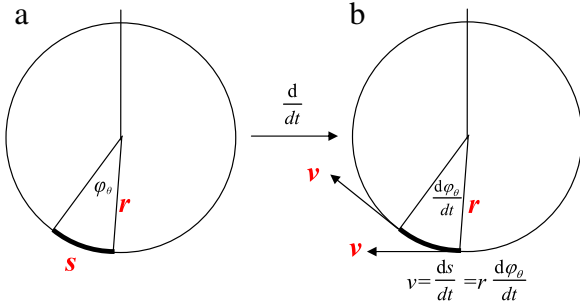


Fig. A.1. Calculation of curve length and linear speed based on angle and angular velocity.

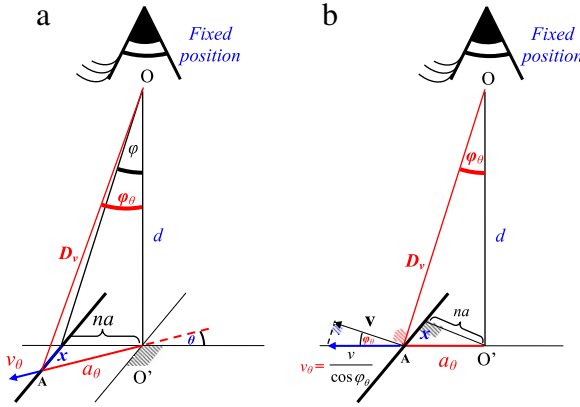


Fig. A.2. No aperture problem assumption. An arbitrary point A over one of the parallel lines with the coordinate (na, x) is selected. The visual angle φ_θ which subtends $O'A$ (point O is the center of stimulus) is used for calculating of the angular speed of point A. In the lack of aperture problem, the real motion of A which is a radial one along OA or a_θ can be registered by motion detectors. In panel (b), the triangle OAA' from panel (a) is laid flat on the page to facilitate the intuition of analysis in Eqs. (A.4)–(A.5).

Combining (A.1) and (A.2) yields:

$$\frac{d\varphi_\theta}{dt} = \frac{n \cdot v \cos^2 \varphi_\theta}{d \cos \theta}. \quad (\text{A.3})$$

With the no aperture problem assumption, to obtain v_θ (Fig. 3), the detectable true motion of each line can be obtained by multiplying $\frac{d\varphi_\theta}{dt}$ with $\frac{D_v}{\cos \varphi_\theta}$, in which D_v is the distance of the target point A from the eye nodal point O:

$$v_\theta = \frac{d\varphi_\theta}{dt} \frac{D_v}{\cos \varphi_\theta}.$$

To prove this by the projection line analysis, two steps are needed by starting from the angular speed $\frac{d\varphi_\theta}{dt}$ to reach to the perceived speed. As Fig. A.1 shows, to obtain the linear speed \mathbf{v} orthogonal to the projection line based on the $s = r\varphi_\theta$ (Fig. A.1(a)), both sides should be differentiated: $v = \frac{ds}{dt} = r \frac{d\varphi_\theta}{dt}$ (Fig. A.1(b)).

As Fig. A.2(a) shows, in the present case, $r = D_v$, therefore:

$$v = \frac{d\varphi_\theta}{dt} D_v. \quad (\text{A.4})$$

In Fig. A.2(b), the triangle with the sides D_v , a_θ , and d (triangle OAA') is laid flatly over the page plane for clarity. As can be seen, motion vector \mathbf{v} obtained by $D_v \frac{d\varphi_\theta}{dt}$ is perpendicular to D_v and hence is not representing the projection line-end velocity over the stimulus plane. The reason v is not flat over the screen stems from the simple geometrical fact that D_v (OA) is not perpendicular to the stimulus plane (except when A is coinciding O, the center of the stimulus).

Obtained speed vector \mathbf{v} (Fig. A.2(b)) makes angle φ_θ with the stimulus plane and v_θ , hence, $v_\theta \cos \varphi_\theta = v$, or $v_\theta = \frac{v}{\cos \varphi_\theta}$.

By replacing v in the latter, using (A.4), we obtain:

$$v_\theta = \frac{d\varphi_\theta}{dt} \frac{D_v}{\cos \varphi_\theta}, \quad (\text{A.5})$$

which completes the proof.

As can be in Fig. A.2(b), $D_v = \frac{d}{\cos \varphi_\theta}$, by replacing this value of D_v in (A.5), we get:

$$v_\theta = \frac{d}{\cos^2 \varphi_\theta} \frac{d\varphi_\theta}{dt}. \quad (\text{A.6})$$

Using (A.3) to replace $\frac{d\varphi_\theta}{dt}$ in (A.6), one obtains:

$$v_\theta = \frac{nv}{\cos \theta}. \quad (\text{A.7})$$

By having v_θ , we can obtain the component of motion perpendicular to line orientation (v_\perp):

$$v_\perp = v_\theta \cos \theta = \frac{nv}{\cos \theta} \cos \theta = nv,$$

which is identical to the original stimulus speed.

We can summarize the above result by the following statement:

With no aperture problem assumption, the projection line analysis yields no illusory distortion and the expansion/contraction of the grating is governed by:

$$v_\perp = nv f^{no}(n, x),$$

in which, the distortion function for the no aperture problem $f^{no}(n, x)$ equals 1.

This shows that for the 3D aperture problem to take place, the 2D aperture problem is needed. This is the topic of the following Appendix B.

Appendix B. Obtaining v_\perp assuming the 2D aperture problem

To derive the distortion function with the aperture problem assumption (f^{Ap}), one can start by differentiating from the both sides of (2) in terms of t (noting that x is constant over time, because due to the aperture problem assumption movement along the line is not detectable):

$$\frac{dtg\varphi_\theta}{dt} = \frac{1}{d} \frac{d}{dt} \left(\sqrt{n^2 a^2 + x^2} \right). \quad (\text{B.1})$$

Using the chain rule $\left(\frac{dtg\varphi_\theta}{dt} = \frac{1}{\cos^2 \varphi_\theta} \frac{d\varphi_\theta}{dt} \right)$ and the fact that $\frac{dx}{dt} = 0$, $\frac{da}{dt} = v$, (B.1) can be rewritten as:

$$\frac{1}{\cos^2 \varphi_\theta} \frac{d\varphi_\theta}{dt} = \frac{n^2 av}{d \sqrt{n^2 a^2 + x^2}}, \quad (\text{B.2})$$

and therefore,

$$\frac{d\varphi_\theta}{dt} = nv \frac{na}{d \sqrt{n^2 a^2 + x^2}} \cos^2 \varphi_\theta. \quad (\text{B.3})$$

Remark. Given $\cos \theta = \frac{na}{\sqrt{n^2 a^2 + x^2}}$ (see Fig. 3), (B.3) can be rewritten as:

$$\frac{d\varphi_\theta}{dt} = \frac{nv}{d} \cos \theta \cos^2 \varphi_\theta. \quad (\text{B.4})$$

This equation highlights better the difference with (A.3), its equivalent with no aperture problem assumption $\left(\frac{d\varphi_\theta}{dt} = \frac{n \cdot v \cos^2 \varphi_\theta}{d} \right)$ by a

factor of $\cos \theta$. This difference explicitly shows that under the aperture problem assumption, we should expect a different value for v_{\perp} rather than nv (which was the case with the no aperture problem assumption). In the following we show that v_{\perp} can be obtained from $\frac{d\varphi_{\theta}}{dt}$ by the following transformation:

$$v_{\perp} = \frac{d\varphi_{\theta}}{dt} f^{\varphi}(n, x),$$

in which,

$$f^{\varphi}(n, x) = \frac{\sqrt{n^2 a^2 + d^2} \sqrt{x^2 + n^2 a^2 + d^2}}{d}.$$

To prove this, we note that in (A.5) for obtaining v_{θ} from $\frac{d\varphi_{\theta}}{dt}$ the latter was multiplied by $\frac{D_v}{\cos \varphi_{\theta}}$. Here, although the multiplication by D_v for the same reason remains, instead, the divisive term $\frac{1}{\cos \varphi_{\theta}}$ should be replaced by $\frac{1}{\cos \varphi}$ to incorporate the 2D aperture problem assumption. This is because only the vertical (or 2D aperture) component of motion (shown by the dotted region in Fig. 6(a)) can be registered, therefore:

$$v_{\perp} = \frac{d\varphi_{\theta}}{dt} \frac{D_v}{\cos \varphi}. \quad (\text{B.5})$$

Again, (B.5) reflects the stage in which the 3D aperture problem kicks in, where the projection line is not orthogonal to the stimulus line.

Regarding $D_v = \frac{d}{\cos \varphi_{\theta}}$ (where $\cos \varphi_{\theta} = \frac{d}{\sqrt{x^2 + n^2 a^2 + d^2}}$), and $\cos \varphi = \frac{d}{\sqrt{n^2 a^2 + d^2}}$ (Fig. 3), one can re-write (B.5) as the following:

$$v_{\perp} = \frac{d\varphi_{\theta}}{dt} \frac{\sqrt{n^2 a^2 + d^2} \sqrt{x^2 + n^2 a^2 + d^2}}{d}. \quad (\text{B.6})$$

Replacing the value of $\frac{d\varphi_{\theta}}{dt}$ from (B.3) in (B.6) results in:

$$v_{\perp} = nv f^{\text{Ap}}(n, x), \quad (\text{B.7})$$

in which,

$$f^{\text{Ap}}(n, x) = \frac{na \sqrt{n^2 a^2 + d^2}}{\sqrt{n^2 a^2 + x^2} \sqrt{x^2 + n^2 a^2 + d^2}}, \quad (\text{B.8})$$

and f^{Ap} indicates the distortion function under the aperture problem assumption. Occasionally, instead of using the abbreviation v_{\perp} we use $v_{\perp}(n, x)$, which emphasizes the coordinate x of the targeted point A over the n th line for which v_{\perp} is obtained.

References

- Adelson, E., & Movshon, J. (1982). Phenomenal coherence of moving visual patterns. *Nature*, 300, 523–525.
- Caplovitz, G. P., Paymer, N. A., et al. (2008). The drifting edge illusion: a stationary edge abutting an oriented drifting grating appears to move because of the 'other aperture problem'. *Vision Research*, 48(22), 2403–2414.
- Fantoni, C., & Pinna, B. (2008). Apparent motion by edge discontinuities. *Perception*, 37(7), 973–992.
- Fennema, C. L., & Thompson, W. B. (1979). Velocity determination in scenes containing several moving objects. *Computer Graph, Image Processing*, 9, 301–315.
- Fermuller, C., Pless, R., et al. (1997). Families of stationary patterns producing illusory movement: insights into the visual system. *Proceedings of the Biological Science*, 264(1383), 795–806.
- Foster, C., & Altschuler, E. L. (2001). The bulging grid. *Perception*, 30(3), 393–395.
- Gong, S., & Brady, M. (1990). Parallel computation of optic flow. *Lecture Notes in Computer Science*, 427, 124–133.
- Gori, S., & Giora, E. et al. (2011). A new motion illusion based on competition between two kinds of motion processing units: the accordion-grating. *Neural Networks*, in this issue (doi: 10.1016/j.neunet.2011.06.017).
- Gori, S., & Hamburger, K. (2006). A new motion illusion: the Rotating-Tilted-Lines illusion. *Perception*, 35(6), 853–857.
- Gori, S., & Yazdanbakhsh, A. (2008). The riddle of the Rotating-Tilted-Lines illusion. *Perception*, 37(4), 631–635.
- Grossberg, S. (2000). Linking mind to brain: the mathematics of biological intelligence. *Notices of the American Mathematical Society*, 47, 1361–1372.
- Grossberg, S., & Mingolla, E. (1993). Neural dynamics of motion perception: direction fields, apertures, and resonant grouping. *Perception & Psychophysics*, 53(3), 243–278.
- Gurnsey, R., Sally, S. L., et al. (2002). Optimising the Pinna–Brelstaff illusion. *Perception*, 31(10), 1275–1280.
- Hildreth, E. C. (1984). The computation of the velocity field. *Proceedings of the Royal Society of London. Series B: Biological Sciences*, 221(1223), 189–220.
- Lorenceanu, J., Shiffrar, M., et al. (1993). Different motion sensitive units are involved in recovering the direction of moving lines. *Vision Research*, 33(9), 1207–1217.
- Pack, C. C., & Born, R. T. (2001). Temporal dynamics of a neural solution to the aperture problem in visual area MT of macaque brain. *Nature*, 409(6823), 1040–1042.
- Spillmann, L. (2009). Phenomenology and neurophysiological correlations: two approaches to perception research. *Vision Research*, 49(12), 1507–1521.
- Stumpf, P. (1911). Über die Abhängigkeit der visuellen Bewegungsrichtung und negativen Nachbildes von den Reizvorgängen auf der Netzhaut. *Zeitschrift für Psychologie*, 59, 321–330.
- Wallach, H. (1935). Über visuell wahrgenommene Bewegungsrichtung. *Psychologische Forschung*, 20, 325–380.
- Weiss, Y., & Adelson, E. H. (2000). Adventures with gelatinous ellipses—constraints on models of human motion analysis. *Perception*, 29(5), 543–566.
- Yazdanbakhsh, A., & Gori, S. (2008). A new psychophysical estimation of the receptive field size. *Neuroscience Letters*, 438(2), 246–251.